GEOPHYSICS, VOL. 50, NO. 5 (MAY 1985); P. 798–809, 12 FIGS.

Integral equation solution for the transient electromagnetic response of a three-dimensional body in a conductive half-space

William A. SanFilipo* and Gerald W. Hohmann‡

ABSTRACT

The time-domain integral equation for the three-dimensional vector electric field is formulated as a convolution of the scattering current with the tensor Green's function. The convolution integral is divided into a sum of integrals over successive time steps, so that a numerical scheme can be formulated with a time stepping approximation of the convolution of past values of the solution with the system impulse response. This, together with spatial discretization, leads to a matrix equation in which previous solution vectors are multiplied by a series of matrices and fed back into the system by adding to the primary field source vector.

The spatial discretization, based on a modification of the usual pulse basis formulation in the frequency domain, includes an additional subset of divergence-free basis functions generated by integrating the Green's function around concentric closed rectangular paths. The inductive response of the body is more accurately modeled with these additional basis functions, and a meaningful solution can be obtained for a body in free space. The resulting algorithm produces good results even for large conductivity contrasts.

Internal checks, including convergence with respect to spatial and temporal discretization, and reciprocity, demonstrate self-consistency of the numerical scheme. Independent checks include (a) comparison with results computed for a prism in free space, (b) comparison with results computed for a thin plate, (c) comparison of our conductive half-space algorithm with an asymptotic solution for a sphere, and (d) comparison with results from inverse Fourier transformation of values computed using a frequency-domain integral equation algorithm.

Qualitative features of the results show that the relative importance of current channeling and confined eddy currents induced in the body depends upon both conductivity contrast and geometry. If the free-space time constant is less than the time window during which currents in the host have not yet propagated well beyond the body, current channeling dominates the response. In such cases, simple superposition of free-space results and the background is a poor approximation. In cases where the host currents diffuse beyond the body in a time less than the free-space time constant of the body, the total response is approximately the sum of the free-space and background (half-space) responses.

INTRODUCTION

Time-domain electromagnetic (TEM) techniques have recently become popular in exploration for minerals, oil, and geothermal resources (Nabighian, 1984). However, theoretical interpretation aids are still quite primitive. Existing numerical solutions include those for thin-plate conductors in free space (Annan, 1974), two-dimensional (2-D) finite-difference schemes (Kuo and Cho, 1980; Goldman and Stoyer, 1983; Oristaglio and Hohmann, 1984), infinite half-planes in free space (Weidelt, 1983), and an asymptotic solution for a sphere in a layered host (Lee, 1981).

To provide a means for calculating the responses of more general three-dimensional (3-D) models, we developed a direct integral-equation solution for the transient response of a prismatic body of conductivity σ_b in a half-space of conductivity σ_* excited by a horizontal rectangular loop of constant current shut off linearly over a short time interval. The derivation of the time-domain integral equation begins with the corresponding frequency-domain derivation of Hohmann (1975) and Hohmann (1983). The advantage of an integral-equation solution over a differential-equation solution is that only the region of anomalous conductivity need be discretized, because the scattering current $\mathbf{j}^s = (\sigma_b - \sigma_*)\mathbf{e}$, where $\mathbf{e}$ is the total vector electric field, is zero outside the body, and the influence of currents in the host is incorporated using the tensor Green's function. However, a convolution integral in time enters into the equation.

The problem of the bimodal nature of the electric tensor Green's function, regarding the dominance of the scalar potential (charge) term over the vector potential (inductive) term, was discussed by Annan (1974) and Lajoie and West (1976). We

Manuscript received by the Editor April 19, 1984; revised manuscript received October 24, 1984.
*CRA Exploration Pty. Ltd., 1030 Anderson Road, Karratha, W.A. 6714, Australia.
‡Department of Geology and Geophysics, University of Utah, Salt Lake City, Utah 84112.

solve this problem by incorporating a specialized subset of basis functions formed by constructing closed eddy-current paths that are divergence free. Application of the Galerkin method results in a pair of coupled equations to solve for the coefficients of divergence-free and pulse basis functions.

The secondary emf(electromotive force)/unit area ($d\mathbf{B}/dt$) at a receiver is obtained from the convolution integral in space and time of the scattering currents with a magnetic tensor Green's function.

THEORETICAL DEVELOPMENT

The electromagnetic (EM) field due to an impressed current $\mathbf{j}^p$ is described by Maxwell's equations:

$$\nabla \times \mathbf{e} = -\mu \frac{\partial \mathbf{h}}{\partial t}$$

$$\nabla \times \mathbf{h} = \sigma \mathbf{e} + \varepsilon \frac{\partial \mathbf{e}}{\partial t} + \mathbf{j}^p.$$

If we ignore displacement currents and assume that $\mu = \mu_0$ everywhere, we can obtain the following vector diffusion equation for the electric field:

$$\nabla \times \nabla \times \mathbf{e} + \mu_0 \sigma \frac{\partial \mathbf{e}}{\partial t} = -\mu_0 \frac{\partial \mathbf{j}^p}{\partial t}.$$

In the frequency domain, assuming an $e^{i\omega t}$ time dependence, we have

$$\nabla \times \nabla \times \mathbf{E} + i\omega\mu_0 \sigma \mathbf{E} = -i\omega\mu_0 \mathbf{J}^p.$$

The general frequency-domain integral equation for the total vector electric field $\mathbf{E}$, composed of a primary (half-space) field $\mathbf{E}^p$ perturbed by a secondary field $\mathbf{E}^s$ from a confined body with conductivity σ_b in a homogeneous host medium of conductivity σ_*, is written symbolically (Hohmann, 1975; Raiche, 1974; Wiedelt, 1975)

$$\mathbf{E}(\mathbf{r}, \omega) = \mathbf{E}^p(\mathbf{r}, \omega) + \sigma_a \int_v \mathbf{G}(\mathbf{r}, \mathbf{r}', \omega)\mathbf{E}(\mathbf{r}', \omega)\, dv', \qquad (1)$$

where $\mathbf{G}$ is the half-space tensor Green's function relating the three vector components of the electric field at $\mathbf{r}$ to the three vector components of an impressed current element at $\mathbf{r}'$ oscillating in time at angular frequency ω. The anomalous conductivity $\sigma_a = \sigma_b - \sigma_*$ is the difference between the conductivities of the scattering body and the host. The Green's function can be broken into two parts: (1) the spatial impulse response in a homogeneous conductive whole space (particular solution to the vector wave equation with a delta function source-current distribution), and (2) the solution to the homogeneous (source-free) vector wave equation that satisfies the boundary conditions at the air-earth interface.

The corresponding integral equation for a transient response requires convolution in time over past values of the scattering current with the retarded tensor Green's function g:

$$\mathbf{e}(\mathbf{r}, t) = \mathbf{e}^p(\mathbf{r}, t) + \sigma_a \int_0^t \int_v g(\mathbf{r}, \mathbf{r}', t - t')\mathbf{e}(\mathbf{r}', t')\, dv'\, dt', \qquad (2)$$

with the initial conditions $\mathbf{e}(\mathbf{r}, t) = 0$ for $t \leq 0$.

The retarded tensor Green's function g is the causal solution of the following parabolic partial differential equation:

$$\nabla \times \nabla \times g(\mathbf{r}, t) + \mu_0 \sigma_* \frac{\partial g(\mathbf{r}, t)}{\partial t} = -\mu_0 \underline{\mathbf{I}}\, \delta(\mathbf{r}, t),$$

where $\underline{\mathbf{I}}$ is the identity tensor.

The scattered electric field $\mathbf{e}^s = \mathbf{e} - \mathbf{e}^p$ can be expressed in terms of a vector potential $\mathbf{a}$ and the gradient of a scalar potential v, for the whole-space solution, plus terms satisfying boundary conditions at the air-earth interface with a secondary tensor Green's function g^s:

$$\mathbf{e}^s(\mathbf{r}, t) = -\mu_0 \frac{\partial}{\partial t} \mathbf{a}(\mathbf{r}, t) - \nabla v(\mathbf{r}, t) + \int_0^t \int_v g^s(\mathbf{r}, \mathbf{r}', t - t')\mathbf{j}^s(\mathbf{r}', t')\, dv'\, dt'. \qquad (3)$$

Using the frequency-domain expressions given in Harrington (1968) and ignoring displacement currents, we can write

$$\mathbf{a}(\mathbf{r}, t) = \int_0^t \int_v \mathbf{j}^s(\mathbf{r}', t')g(\mathbf{r}, \mathbf{r}', t - t')\, dv'\, dt', \qquad (4)$$

and

$$v(\mathbf{r}, t) = -\frac{1}{\sigma_*} \int_0^t \int_v \nabla \cdot \mathbf{j}^s(\mathbf{r}', t')g(\mathbf{r}, \mathbf{r}', t - t')\, dv'\, dt', \qquad (5)$$

where $\mathbf{j}^s = \sigma_a \mathbf{e}$ is the scattering current, and $g(\mathbf{r}, \mathbf{r}'; t - t')$ is the Green's function for the scalar diffusion equation

$$\nabla^2 g - \mu_0 \sigma_* \frac{\partial g}{\partial t} = \mu_0\, \delta(\mathbf{r}, t),$$

given by

$$g(\mathbf{r}, \mathbf{r}', t) = \frac{1}{4\pi^{3/2}}\, \theta W(R),$$

with

$$\theta = \left(\frac{\mu_0 \sigma_*}{4t}\right)^{1/2},$$

$$W(R) = \exp\left(-\theta^2 R^2\right)/t,$$

and

$$R^2 = (x - x')^2 + (y - y')^2 + (z - z')^2.$$

Equation (2) is the symbolic representation of equations (3), (4), and (5).

The secondary tensor Green's function g^s is found by inverse Laplace transformation of the corresponding frequency-domain secondary tensor Green's function. Using the

frequency-domain expressions presented in Hohmann (1975), we obtain

$$g^e(\mathbf{r}, \mathbf{r}', t - t') = \begin{bmatrix} \frac{\partial}{\partial x'}(x - x')\alpha_1 + \alpha_2 & \frac{\partial}{\partial y'}(x - x')\alpha_1 & \frac{\partial}{\partial z'}(x - x')\alpha_3 \\ \frac{\partial}{\partial x'}(y - y')\alpha_1 & \frac{\partial}{\partial y'}(y - y')\alpha_1 + \alpha_2 & \frac{\partial}{\partial z'}(y - y')\alpha_3 \\ \frac{\partial}{\partial x'}(z + z')\alpha_3 & \frac{\partial}{\partial y'}(z + z')\alpha_3 & \frac{\partial}{\partial z'}(z + z')\alpha_3 + \alpha_4, \end{bmatrix}$$

with

$$\alpha_1 = \mathscr{L}^{-1}\left\{\frac{1}{4\pi\sigma_* r}\int_0^\infty \left(2 - \frac{\lambda}{u}\right)e^{-u(z+z')}\lambda J_1(\lambda r)d\lambda\right\}$$

$$= \frac{1}{2\pi^{3/2}\sigma_*}\left\{\frac{z + z'}{r}\theta^3 W(z + z') \times \int_0^\infty \beta e^{-\beta^2/4}J_1(\beta\rho)\,d\beta - \theta^3 W(R_1)\right\},$$

$$\alpha_2 = \mathscr{L}^{-1}\left\{\frac{k^2}{4\pi\sigma_*}\int_0^\infty \frac{u - \lambda}{u + \lambda}\frac{\lambda}{u}e^{-u(z+z')}J_0(\lambda r)\,d\lambda\right\}$$

$$= \frac{\theta^3}{2\pi^{3/2}\sigma_*}\left\{\theta(z + z')W(z + z')\int_0^\infty \beta^2 e^{-\beta^2/4}J_0(\beta\rho)\,d\beta - \tfrac{1}{4}W(z + z')\int_0^\infty \beta^3 e^{-\beta^2/4}J_0(\beta\rho)\,d\beta + (1 - 2\theta^2(z + z')^2)W(R_1)\right\},$$

$$\alpha_3 = \mathscr{L}^{-1}\left\{\frac{ikR_1 + 1}{4\pi\sigma_* R_1^3}\exp(-ikR_1)\right\}$$

$$= \frac{1}{2\pi\sigma_*}\theta^3 W(R_1),$$

and

$$\alpha_4 = \mathscr{L}^{-1}\left\{\frac{k^2}{4\pi\sigma_* R_1}\exp(-ikR_1)\right\}$$

$$= -\mu_0\frac{\partial}{\partial t}g(R_1, t),$$

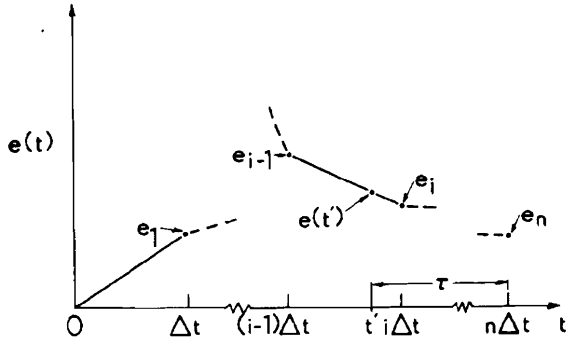

FIG. 1. Linear approximation of the electric field during an interval $(i - 1)\Delta t \le t' \le i\Delta t$.

where $\mathscr{L}^{-1}$ denotes inverse Laplace transformation, and with the horizontal distance $\mathbf{r} = [(x - x')^2 + (y - y')^2]^{1/2}$, the image distance $R_1 = [r^2 + (z + z')^2]^{1/2}$, the dimensionless horizontal distance $\rho = \theta r$, and $u = (\lambda^2 - k^2)^{1/2}$.

The inverse Laplace transforms of the terms expressed as Hankel transforms are obtained by using the shifted frequency $\omega' = \omega - i\lambda^2/\mu_0\sigma_*$ and shifted wavenumber $k' = (-i\omega'\mu_0\sigma_*)^{1/2}$. Then we manipulate individual terms in the kernel functions so that the same form as that of the scalar Green's functions above, or a derivative of it, is obtained, and the same Laplace transform relation can be used. Further simplification results if the variable changes $\rho = \theta r$ and $\beta = \lambda/\theta$ are made. Some of the resulting Hankel transforms have closed-form solutions (Gradshteyn and Ryzhik, 1965).

NUMERICAL SOLUTION

Time stepping the convolution integral

Solving equation (2) does not require solving for $\mathbf{e}(\mathbf{r}, t)$ for all times simultaneously; causality allows a time-stepping procedure in which the fields are zero for all times before $t = 0$, when the current in the transmitter begins to shut off. We approximate the time evolution of the electric field for $t > 0$ with a continuous piece-wise linear function over successive time intervals of equal duration Δt (Figure 1).

Explicit spatial dependences are omitted until the following section by using the expressions:

$$\tilde{\mathbf{g}}(t - t')\mathbf{e}(t') = \sigma_a\int_v g(\mathbf{r}, \mathbf{r}', t - t')\mathbf{e}(\mathbf{r}', t')\,dv',$$

and

$$\mathbf{e}_n = \mathbf{e}(\mathbf{r}, n\Delta t).$$

Then rewriting equation (2), we have

$$\mathbf{e}_n = \mathbf{e}_n^p + \sum_{i=1}^{n}\int_{(i-1)\Delta t}^{i\Delta t}\tilde{\mathbf{g}}(t - t')\mathbf{e}(t')\,dt'. \tag{6}$$

To derive a system of equations involving the values at the sample $i\Delta t$, we express $\mathbf{e}(t')$ in terms of the sample values $\{\mathbf{e}_i\}_1^n$. During the interval $(i - 1)\Delta t \le t' \le i\Delta t$ (Figure 1), we have

$$\mathbf{e}(t') = \mathbf{e}_i - \frac{\tau - (n - i)\Delta t}{\Delta t}(\mathbf{e}_i - \mathbf{e}_{i-1})$$

$$= (n - i + 1)\mathbf{e}_i - (n - i)\mathbf{e}_{i-1} - \frac{\tau}{\Delta t}\mathbf{e}_i + \frac{\tau}{\Delta t}\mathbf{e}_{i-1}, \tag{7}$$

where $\tau = n\Delta t - t'$. Substituting equation (7) into equation (6) gives

$$\mathbf{e}_n = \mathbf{e}_n^p + \sum_{i=1}^{n}(n-i+1)\mathbf{e}_i \int_{(n-i)\Delta t}^{(n-i+1)\Delta t} g(\tau)\,d\tau - \sum_{i=1}^{n}(n-i)\mathbf{e}_{i-1}\int_{(n-i)\Delta t}^{(n-i+1)\Delta t} \underset{\sim}{\hat{\mathbf{g}}}(\tau)\,d\tau - \sum_{i=1}^{n}\frac{\mathbf{e}_i}{\Delta t}\int_{(n-i)\Delta t}^{(n-i+1)\Delta t}\tau\underset{\sim}{\hat{\mathbf{g}}}(\tau)\,d\tau + \sum_{i=1}^{n}\frac{\mathbf{e}_{i-1}}{\Delta t}\int_{(n-i)\Delta t}^{(n-i+1)\Delta t}\tau\underset{\sim}{\hat{\mathbf{g}}}(\tau)\,d\tau. \tag{8}$$

Collecting coefficients of each $\mathbf{e}_i$ up to and including the unknown value $\mathbf{e}_n$ and applying the initial condition $\mathbf{e}_0 = 0$ gives

$$\mathbf{e}_n = \mathbf{e}_n^p + \sum_{j=1}^{n-1}\underset{\sim}{\Gamma}_j\mathbf{e}_{n-j} + \underset{\sim}{\Gamma}_0\mathbf{e}_n, \tag{9}$$

$$\Gamma_j = (j+1)\int_{j\Delta t}^{(j+1)\Delta t}\underset{\sim}{\hat{\mathbf{g}}}(\tau)\,d\tau - (j-1)\int_{(j-1)\Delta t}^{j\Delta t}\underset{\sim}{\hat{\mathbf{g}}}(\tau)\,d\tau - \frac{1}{\Delta t}\int_{j\Delta t}^{(j+1)\Delta t}\tau\underset{\sim}{\hat{\mathbf{g}}}(\tau)\,d\tau + \frac{1}{\Delta t}\int_{(j-1)\Delta t}^{j\Delta t}\tau\underset{\sim}{\hat{\mathbf{g}}}(\tau)\,d\tau, \tag{10a}$$

and

$$\Gamma_0 = \int_0^{\Delta t}\underset{\sim}{\hat{\mathbf{g}}}(\tau)\,d\tau - \frac{1}{\Delta t}\int_0^{\Delta t}\tau\underset{\sim}{\hat{\mathbf{g}}}(\tau)\,d\tau. \tag{10b}$$

These expressions simplify for the whole-space vector potential operator [first term in equation (3)]. Integrating out the time derivative in the first two terms in equation (10a) and integrating by parts the last two terms [or first term and last term of equation (10b)] gives

$$\underset{\sim}{\Gamma}_j^a = (j+1)\int_{j\Delta t}^{(j+1)\Delta t} -\mu_0\frac{\partial}{\partial\tau}\underset{\sim}{\hat{\mathbf{g}}}(\tau)\,d\tau - (j-1)\int_{(j-1)\Delta t}^{j\Delta t} -\mu_0\frac{\partial}{\partial\tau}\underset{\sim}{\hat{\mathbf{g}}}(\tau)\,d\tau - \frac{1}{\Delta t}\int_{j\Delta t}^{(j+1)\Delta t}\tau\left[-\mu_0\frac{\partial}{\partial\tau}\underset{\sim}{\hat{\mathbf{g}}}(\tau)\right]d\tau + \frac{1}{\Delta t}\int_{(j-1)\Delta t}^{j\Delta t}\tau\left[-\mu_0\frac{\partial}{\partial\tau}\underset{\sim}{\hat{\mathbf{g}}}(\tau)\right]d\tau,$$

or

$$\underset{\sim}{\Gamma}_j^a = \mu_0\Bigg\{(j+1)[\underset{\sim}{\hat{\mathbf{g}}}(j\Delta t) - \underset{\sim}{\hat{\mathbf{g}}}(j+1)\Delta t)] + (j-1)[\underset{\sim}{\hat{\mathbf{g}}}(j\Delta t) - \underset{\sim}{\hat{\mathbf{g}}}((j-1)\Delta t)] + \Bigg[(j+1)\underset{\sim}{\hat{\mathbf{g}}}((j+1)\Delta t) - j\underset{\sim}{\hat{\mathbf{g}}}(j\Delta t) - \frac{1}{\Delta t}\int_{j\Delta t}^{(j+1)\Delta t}\underset{\sim}{\hat{\mathbf{g}}}(\tau)\,d\tau\Bigg] + \Bigg[(j-1)\underset{\sim}{\hat{\mathbf{g}}}((j-1)\Delta t) - j\underset{\sim}{\hat{\mathbf{g}}}(j\Delta t) + \frac{1}{\Delta t}\int_{(j-1)\Delta t}^{j\Delta t}\underset{\sim}{\hat{\mathbf{g}}}(\tau)\,d\tau\Bigg]\Bigg\}$$

$$= \frac{\mu_0}{\Delta t}\left\{\int_{(j-1)\Delta t}^{j\Delta t}\underset{\sim}{\hat{\mathbf{g}}}(\tau)\,d\tau - \int_{j\Delta t}^{(j+1)\Delta t}\underset{\sim}{\hat{\mathbf{g}}}(\tau)\,d\tau\right\}. \tag{11a}$$

Similarly, we obtain

$$\underset{\sim}{\Gamma}_0^a = -\frac{\mu_0}{\Delta t}\int_0^{\Delta t}\underset{\sim}{\hat{\mathbf{g}}}(\tau)\,d\tau, \tag{11b}$$

with

$$\underset{\sim}{\hat{\mathbf{g}}}(\tau) = \int_v g(\mathbf{r}, \mathbf{r}', \tau)\,dv'.$$

Except for the terms with Hankel transform expressions, the integrals in equations (10) and (11) can be carried out analytically and are expressed in series form as incomplete gamma functions.

Spatial discretization

We now treat the method of discretization of the spatial dependence of equation (2) to arrive at a numerical scheme represented by a matrix equation. Because of the complexity of the full 3-D problem, a simple scheme is required, so we start with pulse basis functions over rectangular prismatic cells built out of cubic subcells (Wannamaker et al., 1984). We then add a specialized subset of basis functions that have only inductive coupling, constructed out of the same prismatic cells used for the pulse basis functions. The method of moments (Harrington, 1968) is applied using the same set of functions for weighting functions as used for the basis functions (Galerkin method). The usual point-matching method is not meaningful for vector (current-tube) basis functions, and the Galerkin method eliminates the large scalar-potential operator from one of the resulting coupled integral equations.

At time $t = n\Delta t$, the electric field at any point in the body $\mathbf{e}(\mathbf{r}, n\Delta t)$ is approximated with a linear combination of pulse and divergence-free basis functions, denoted $p_i(\mathbf{r})$ and $\mathbf{e}_i^c(\mathbf{r})$, respectively. Then we have

$$\mathbf{e}(\mathbf{r}, n\Delta t) \approx \sum_{i=1}^{N}\mathbf{e}_i^0\,p_i(\mathbf{r}) + \sum_{i=1}^{M}c_i\mathbf{e}_i^c(\mathbf{r}). \tag{12}$$

The body is divided into N cells and M rectangular closed tubes as shown in Figure 2, and the basis functions are defined as

$$p_i(\mathbf{r}) = \begin{cases}1, & \mathbf{r} \text{ in the } i\text{th cell}\\ 0, & \text{otherwise}\end{cases};$$

and

$$\mathbf{e}_i^c(\mathbf{r}) = \begin{cases}\dfrac{\mathbf{u}(\mathbf{r})}{a(\mathbf{r})}, & \mathbf{r} \text{ in the } i\text{th tube}\\ \text{otherwise}\end{cases},$$

where $\mathbf{u}(\mathbf{r})$ is the unit vector in the direction that the current flows in the ith current tube according to the right-hand rule with respect to the coordinate system axis normal to the plane of the current tube (Figure 2), and $a(\mathbf{r})$ is the cross-sectional area of the tube. Note that $a(\mathbf{r})$ changes when the current changes

direction if the cell aspect ratio is not 1. The electric flux, rather than the electric field, is constant within a tube.

The unknown vector coefficients $\mathbf{e}_i^0$ are coupled through equations (3), (4), and (5). Spatial discretization of these equations is accomplished by integrating the Green's functions over the source volumes defined by the pulse basis functions and integrating over the field point volumes defined by the pulse weight functions [taking the inner product of both sides of equation (3) with the weight functions]. The unknown scalar coefficients c_i are coupled through equations (3) and (4), but equation (5) [and thus the second term in equation (3)] makes no contribution, because the scattering current distribution described by $c_i \mathbf{e}_i(\mathbf{r})$ is divergence-free. Cross-coupling between the two types of basis functions also does not have a contribution from the scalar potential term.

Substituting equation (12) into equation (2) gives

$$\sum_{i=1}^{N} \mathbf{e}_i^0 p_i(\mathbf{r}) + \sum_{i=1}^{M} c_i \mathbf{e}_i^c(\mathbf{r}) = \mathbf{e}^p(\mathbf{r}) + \sigma_a \int_v \tilde{\mathbf{g}}(\mathbf{r}, \mathbf{r}') \left[\sum_{i=1}^{N} \mathbf{e}_i^0 p_i(\mathbf{r}') + \sum_{i=1}^{M} c_i \mathbf{e}_i^c(\mathbf{r}') \right] dv', \tag{13}$$

where the tilde over the tensor Green's function indicates that the time integrals in expressions (10) and (11) have been carried out and that $t = n\Delta t$ is the instant in time at which we are solving for the electric fields. The summations in equation (9) are implied.

The Galerkin method is applied using the same two sets of functions given by equation (12) as weighting functions, and we derive two sets of coupled integral equations for the unknown coefficients $\mathbf{e}_i^0$ and c_i. The first equation is

$$\int_v p_j(\mathbf{r}) \left[\sum_{i=1}^{N} \mathbf{e}_i^0 p_i(\mathbf{r}) \right] dv = \mathbf{e}_j^0 \int_v p_j(\mathbf{r})\, dv - \int_v p_j(\mathbf{r}) \mathbf{e}^p(\mathbf{r})\, dv + \sigma_a \int_v p_j(\mathbf{r}) \int_v g(\mathbf{r}, \mathbf{r}') \times \left[\sum_{i=1}^{N} \mathbf{e}_i^0 p_i(\mathbf{r}') + \sum_{i=1}^{M} c_i \mathbf{e}_i^c(\mathbf{r}') \right] dv'\, dv - \int_v p_j(\mathbf{r}) \sum_{i=1}^{M} c_i \mathbf{e}_i^c(\mathbf{r})\, dv.$$

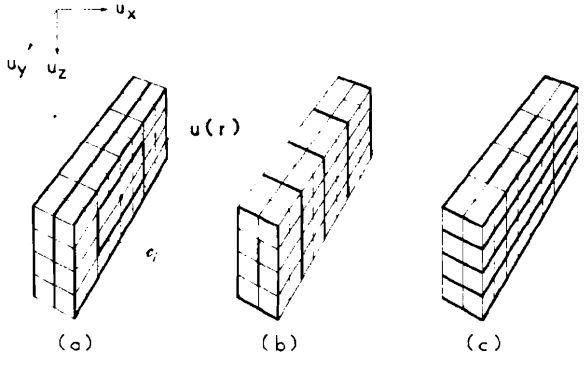

FIG. 2. A prismatic body divided into 32 cells (8 cells/quadrant), each built out of 2 cubic subcells, defining the pulse functions $\{p_i(\mathbf{r})\}_1^N$, and the combinations of cells (outlined by heavy lines) for (a) 4 closed current tubes normal to $\mathbf{u}_x$, (b) 4 normal to $\mathbf{u}_y$, and (c) 4 normal to $\mathbf{u}_z$. An example of a closed integration path c_i with unit direction vector $\mathbf{u}(\mathbf{r})$ is shown in (a).

The terms multiplied by $g(\mathbf{r}, \mathbf{r}')$ involve past values of the electric fields as well as the present, unknown value through the implied summation in equation (9); the other terms only involve the value at $n\Delta t$. Normalizing by the cell volume and rearranging gives

$$\mathbf{e}_j^0 = \frac{1}{v_j} \int_v p_j(\mathbf{r}) \mathbf{e}^p(\mathbf{r})\, dv + \sum_{i=1}^{N} \frac{\mathbf{e}_i^0}{v_j} \int_v \int_v p_j(\mathbf{r}) p_i(\mathbf{r}') \sigma_a \tilde{\mathbf{g}}(\mathbf{r}, \mathbf{r}')\, dv'\, dv + \sum_{i=1}^{M} \frac{c_i}{v_j} \int_v \int_v [\sigma_a \tilde{\mathbf{g}}(\mathbf{r}, \mathbf{r}') - \delta(\mathbf{r} - \mathbf{r}'; n\Delta t - t')] \times p_j(\mathbf{r}) \mathbf{e}_i^c(\mathbf{r}')\, dv'\, dv, \tag{14}$$

where

$$v_j = \int_v p_j(\mathbf{r})\, dv.$$

The second equation is

$$\int_v \mathbf{e}_j^c(\mathbf{r}) \cdot \sum_{i=1}^{M} c_i \mathbf{e}_i^c(\mathbf{r})\, dv = \int_v \mathbf{e}_j^c(\mathbf{r}) \cdot \mathbf{e}^p(\mathbf{r})\, dv + \int_v \mathbf{e}_j^c(\mathbf{r}) \cdot \sigma_a \int_v \sum_{i=1}^{M} \mathbf{e}_i^0 p_i(\mathbf{r}') \tilde{\mathbf{g}}(\mathbf{r}, \mathbf{r}')\, dv'\, dv + \int_v \mathbf{e}_j^c(\mathbf{r}) \cdot \sigma_a \int_v \sum_{i=1}^{M} c_i \mathbf{e}_i^c(\mathbf{r}') \tilde{\mathbf{g}}(\mathbf{r}, \mathbf{r}')\, dv'\, dv - \int_v \mathbf{e}_j^c(\mathbf{r}) \sum_{i=1}^{N} \mathbf{e}_i^0(\mathbf{r}) p_i(\mathbf{r})\, dv.$$

Rearranging and noting that the current-tube basis functions are not mutually orthogonal, we obtain an expression for the coefficients c_i:

$$c_j = \frac{1}{T_j} \int_v \mathbf{e}_j^c(\mathbf{r}) \cdot \mathbf{e}^p(\mathbf{r})\, dv + \sum_{i=1}^{N} \frac{\mathbf{e}_i^0}{T_j} \cdot \int_v \int_v \mathbf{e}_j^c(\mathbf{r}) p_i(\mathbf{r}') [\sigma_a \tilde{\mathbf{g}}(\mathbf{r}, \mathbf{r}') - \delta(\mathbf{r} - \mathbf{r}'; n\Delta t - t')]\, dv'\, dv + \sum_{i=1}^{M} \frac{c_i}{T_j} \int_v \int_v \mathbf{e}_j^c(\mathbf{r}) \cdot \mathbf{e}_i^c(\mathbf{r}') [\sigma_a \tilde{\mathbf{g}}(\mathbf{r}, \mathbf{r}') - \delta_{i \neq j}(\mathbf{r} - \mathbf{r}'; n\Delta t - t')\, dv'\, dv, \tag{15}$$

with

$$T_j = \int_v \mathbf{e}_j^c(\mathbf{r}) \cdot \mathbf{e}_j^c(\mathbf{r})\, dv.$$

The appearance of the delta functions results from the nonorthogonality between the different basis functions and weight functions, with the time dependence indicating they are includ-

ed only in the integrals over the first time step in expressions (10b) and (11b). The spatial integrals over these delta functions contribute whenever basis functions overlap.

The second sums in equations (14) and (15) do not include a scalar potential contribution because the basis functions $\{\mathbf{e}_i^c\}_1^M$ are divergence-free. The first sum in equation (15) also does not require the scalar potential term, because the integral over the unprimed variables includes an integral around a closed path of the dot product of the gradient of a scalar potential with the unit direction vector, which is zero by Stoke's theorem. The only term in which equation (5) must be included is in the first sum in expression (14), representing coupling between the pulse basis functions.

The volume integrals are approximated with evaluations of the Green's functions at the subcell centers, i.e., using a 3-D midpoint rule with the subcell as the volume interval, except for the case when $\mathbf{r}' = \mathbf{r}$. This method is adequate for the R^{-1} behavior of the Green's function. The line integrals associated with the current-tube basis and weight functions are accomplished by combining the contributions from appropriate cells. When the source and field subcells coincide, the integration of the whole-space terms is done analytically by approximating the cubic current (vector potential), or charge [$\nabla \cdot \mathbf{j}^s$ in equation (5)] distribution with an equal-volume sphere.

The vector potential term for the case where $\mathbf{r} = \mathbf{r}'$ is handled by carrying out the time differentiation in equation (3), integrating over the source volume, and using expression (10) instead of expression (11). There is an integrable singularity at $R = 0$ that requires the limiting process used below. Carrying out the time differentiation gives

$$-\mu_0 \frac{\hat{c}}{\partial t} g(\mathbf{r}, \mathbf{r}', t) = \frac{1}{\pi^{3/2}\sigma_*}(\tfrac{3}{2} - \theta^2 R^2)\theta^3 W(R).$$

Integrating over the volume of the subcell, with $(4/3)\pi R_0^3 =$ cubic subcell volume and excluding an infinitesimal spherical region of radius ε (for reasons apparent below), we have

$$\int_0^{2\pi} d\phi \int_0^{\pi} \sin\theta\, d\theta \int_{\varepsilon}^{R_0} \frac{1}{\pi^{3/2}\sigma_*}(\tfrac{3}{2} - \theta^2 R^2)\theta^3 W(R) R^2\, dR = \frac{2}{\sqrt{\pi}\sigma_*}[\theta^3 R_0^3 W(R_0) - \theta^3 \varepsilon^3 W(\varepsilon)].$$

Next we carry out the time integral in expression (10b):

$$\int_0^{\Delta t} \frac{2}{\sqrt{\pi}\sigma_*}[\theta^3 R_0^3 W(R_0) - \theta^3 \varepsilon^3 W(\varepsilon)]\, dt = \frac{2}{\sqrt{\pi}\sigma_*}\left\{R_0^3\left[\frac{\sqrt{\pi}}{2R_0^3} - \theta_0^3 \gamma_{3/2}(\theta_0^2 R_0^2)\right] - \varepsilon^3\left[\frac{\sqrt{\pi}}{2\varepsilon^3} - \theta_0^3 \gamma_{3/2}(\theta_0^2 \varepsilon^2)\right]\right\} = \frac{2}{\sqrt{\pi}\sigma_*}[\theta_0^3 \varepsilon^3 \gamma_{3/2}(\theta_0^2 \varepsilon^2) - \theta_0^3 R_0^3 \gamma_{3/2}(\theta_0^2 R_0^2)],$$

and in the limit $\varepsilon \to 0$ this expression becomes

$$= -\frac{2}{\sqrt{\pi}\sigma_*}\theta_0^3 R_0^3 \gamma_{3/2}(\theta_0^2 R_0^2),$$

where

$$\gamma_\nu(x) = \sum_{n=0}^{\infty} \frac{(-x)^n}{n!(n+\nu)},$$

and

$$\theta_0 = \left(\frac{\mu_0 \sigma_*}{4\Delta t}\right)^{1/2}$$

Note that the term we obtain vanishes in the quasi-static, free-space limit for a finite Δt, as we would expect since the propagation time for the induced field from a step current source would be zero.

The second time integral in expression (10b) does not require the limiting process involving the region about the field point:

$$\frac{2}{\sqrt{\pi}\sigma_*}\theta_0^2 R_0^3 \int_0^{\Delta t} \theta W(R_0)\, dt = \frac{2}{\sqrt{\pi}\sigma_*}\theta_0^2 R_0^2[\sqrt{\pi} - \theta_0^2 R_0^2 \gamma_{1/2}(\theta_0^2 R_0^2)].$$

The first term in this expression does not depend upon σ_* and describes the quasi-static free-space self-inductance of a spherical volume of current changing linearly in time.

The scalar potential (charge) term described by equation (5) is handled in the manner described in Hohmann (1983). The electric charge associated with the divergence of $\mathbf{j}^s$ (fictitious on internal boundaries, but real at the surface of the body) is assumed to be distributed uniformly in a spherical volume equal to that of a cubic subcell and centered at the subcell face. The retarded scalar potential expression (5) is calculated for field points on each side of the cell centered at $\mathbf{r}$ using equation (10) and differenced to approximate the averaged gradient in the field cell. The contribution of $\nabla \cdot \mathbf{j}^s$ for each cell is the normal component of $\mathbf{j}^s$ multiplied by the area of the cell boundary.

This procedure results in a more rapid convergence with respect to spatial discretization than if we use the more standard procedure of calculating the electric field at the field-cell center from a surface charge distribution on the source-cell boundary (Hohmann, 1983). It also eliminates the need to use more than a single point evaluation when carrying out the spatial integrals for adjacent subcells, because of the $1/R$ rather than the $1/R^3$ Green's function.

The addition of the specialized current-tube basis functions provides a basis subset that individually satisfies free-space boundary conditions: current does not leak out of the body and is divergence-free. The inductive coupling between these current tubes is not sensitive to the host conductivity; this feature is appropriate for closed eddy currents induced in a good conductor buried in a very resistive host. The pulse basis functions are well suited for describing the current channeling response of the target. The limitation of the closed current tubes is the geometric constraints placed on the eddy-current distribution. The quasi-static, free-space limit can be approximated by using only the current-tube basis functions, since the matrix elements associated with the pulse basis functions diverge in the free-space limit, requiring the solution vector to become zero.

The resulting system of equations has a temporal description given by expressions (10) and (11) and a spatial description given by expressions (14) and (15). A final partitioned matrix representation is written

$$\left[\begin{array}{c|c} \mathbf{I} - \boldsymbol{\Gamma}_0^{00} & \mathbf{J}^{0c} - \boldsymbol{\Gamma}_0^{0c} \\ \hline \mathbf{J}^{c0} - \boldsymbol{\Gamma}_0^{c0} & \mathbf{J}^{cc} - \boldsymbol{\Gamma}_0^{cc} \end{array}\right] \left[\begin{array}{c} \mathbf{e}_n^0 \\ \hline c_n \end{array}\right] = \left[\begin{array}{c} \mathbf{e}_n^p \\ \hline c_n^p \end{array}\right] + \sum_{j=1}^{n-1} \left[\begin{array}{c|c} \boldsymbol{\Gamma}_j^{00} & \boldsymbol{\Gamma}_j^{0c} \\ \hline \boldsymbol{\Gamma}_j^{c0} & \boldsymbol{\Gamma}_j^{cc} \end{array}\right] \left[\begin{array}{c} \mathbf{e}_{n-j}^0 \\ \hline c_{n-j} \end{array}\right] \tag{16}$$

Here $\boldsymbol{\Gamma}_{i-1}^{00}$ represents the $3N \times 3N$ matrix of coupling coefficients between the pulse basis functions over the ith time step, and $\mathbf{I}$ is the identity matrix. $\boldsymbol{\Gamma}_j^{0c}$ and $\boldsymbol{\Gamma}_j^{c0}$ are the cross-coupling matrices ($M \times 3N$ and $3N \times M$) between the pulse basis functions and the closed current tubes, with $\mathbf{J}^{0c}$ and $\mathbf{J}^{c0}$ the terms associated with the delta functions in equations (14) and (15). $\boldsymbol{\Gamma}_j^{cc}$ is the $M \times M$ matrix of coupling coefficients between the current tubes, with $\mathbf{J}^{cc}$ including the identity matrix and terms from the delta functions in expression (15) that arise when current tubes overlap.

The system of equations (16) must be solved at every time step, with the past solution vectors multiplied by the appropriate matrices and fed back into the source term. This becomes impractical for more than a few tens of time steps. Fortunately, the integral operator is a smoothing operator, so that large time steps can be used without encountering the stability problems of a finite-difference scheme.

A substantial reduction in computer costs is also achieved by incorporating a similarity transformation for bodies with two planes of symmetry as described in Tripp and Hohmann (1984). The transformation block diagonalizes the impedance matrices in representation (16) into four $(3N + M)/4 \times (3N + M)/4$ matrices. By restricting the models to have the transmitting loop lie on one of the symmetry planes, two of the four transformed source vectors vanish and a further reduction in cost is achieved.

Primary fields

The source vector in equation (16) includes the primary (half-space) electric field averaged over each cell (by point sampling at subcell centers), and the primary normalized emf around each current tube weighted by the cross-sectional area (the electric flux, which is the product of the cross-sectional area and the electric field, is the constant represented by the coefficient c_i^p). We calculate the primary electric field by convolving the impulse response for a horizontal current element at the Earth's surface with the current waveform, and integrating around the finite rectangular transmitting loop. The impulse response for an ungrounded current element is the xx component of the inductive terms of the tensor Green's function above, with the induced field parallel to the current element. We approximate the normalized emf by adding up the fields in the appropriate cells and normalizing by T_i in equation (15).

The current waveform consists of a constant current terminated with a finite linear ramp having a duration equal to the time step used in the integral-equation solution. The first sample occurs precisely at the bottom of the current ramp; the finite shut-off time results in primary fields that are smoother in both space and time than they would be for an ideal step-current waveform. This avoids undersampling of the primary fields, particularly when relatively large time steps (i.e., $\theta_0 R \ll 1$) are used.

Secondary emf at receiver position

Having calculated the electric field in the body, we need to determine the time derivative of the secondary magnetic induction ($d\mathbf{B}/dt$) at a receiver site. For finite receiving loops, a numerical integration is used to find the total emf (induced voltage).

We derive a tensor Green's function relating the three components of $d\mathbf{B}/dt$ to a current impulse impressed in a conductive half-space by taking the curl of equation (3). We define the curl of a tensor operator g such that $(\nabla \times g)\mathbf{e} = \nabla \times (g\mathbf{e})$. The curl of the gradient of a scalar potential makes no contribution; the term representing the whole-space vector potential is convolved using expression (11), and $\nabla \times g^s$ is convolved using expression (10). The source volume includes only the anomalous region, where σ_a (and thus $\mathbf{j}^s$) is nonzero.

The primary (half-space) induction at receiver sites is calculated by convolving the magnetic Green's function with the current waveform and integrating numerically around the transmitting loop.

NUMERICAL CHECKS

An essential part of the development of a computer program is verification of its accuracy. Internal checks include spatial and temporal convergence and reciprocity for a pair of horizontal transmitting and receiving loops. Spatial convergence checks for the complete scheme with a conductive half-space are limited because of the rapid increase in computer demands with the number of cells (decreasing the cell size by one-half increases the number of matrix elements in the pulse basis block by a factor of 64). However, a free-space version with only current-tube basis functions, only one feedback term in the convolution, and a much simpler Green's function allows a more extensive convergence check that should test convergence for the half-space scheme.

Figure 3 shows the decay curves of the emf for the coincident-loop (SIROTEM) configuration using three discretizations (given in number of cells in the positive x-y quadrant because of the incorporation of the symmetry transformation) of a cubic body. At early times the finer discretization resolves the higher-order current modes, and the solution has converged at 54 cells/quadrant. Even the crude 16 cells/quadrant approximation is adequate for most purposes.

Insensitivity to the size of the time step is demonstrated in Figure 4, with the 0.1 ms time step giving good results. The time constant for this model is about 0.6 ms, and we observe significant error if the time step is more than 10 to 20 percent of the time constant. This is not surprising considering that we are approximating an exponential decay with a piece-wise linear approximation.

Verification of reciprocity is another important self-check for a numerical modeling algorithm. Numerical techniques for solving integral equations require sampling of the source fields and approximate integration of the scattering current and the magnetic Green's function. The methods employed in sampling the source field and evaluating the scattered fields are not identical, so errors are not reciprocal. Figure 5 shows numerical results computed with our solution are approximately the same if the transmitter and receiver are interchanged. Both the transmitter and receiver are large, square, horizontal loops on the

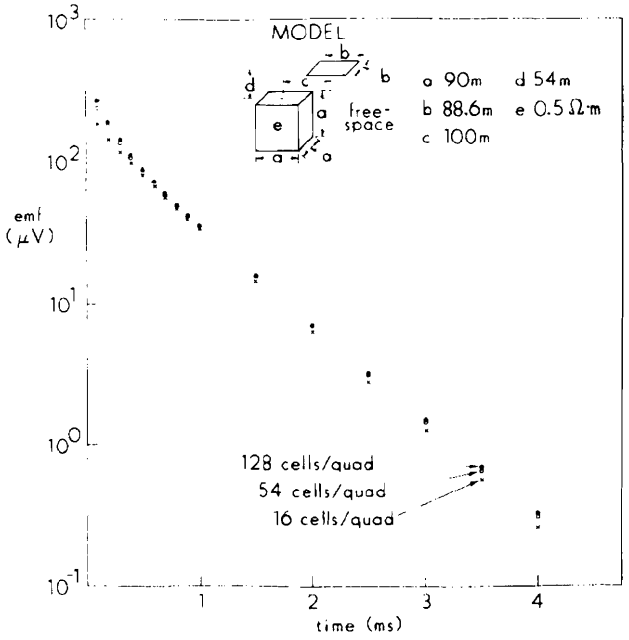

FIG. 3. Spatial convergence check using three discretizations for the free-space response of a conductive cube with a coincident loop system.

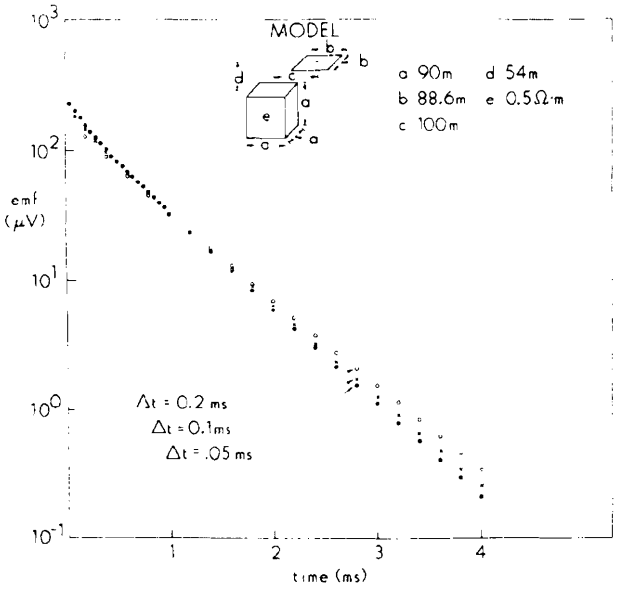

FIG. 4. Temporal convergence check using three time-step sizes for the same model as in Figure 3.

surface of a 100 Ω · m half-space containing a 0.5 Ω · m cubic body that is 90 m on a side.

Internal checks establish self-consistency of our scheme, but checks with independent results using other numerical algorithms or scale-model experiments are more conclusive. We modified the free-space program so that thin plates could be modeled and the results compared with those calculated using Annan's (1974) eigenmode algorithm. Profiles over a vertical dike for both vertical and horizontal components of $d\mathbf{B}/dt$ are compared in Figure 6. The model consists of a 50-S plate 600 m long, 300 m in depth extent, buried 30 m to the top. The source loop is 600 m by 300 m; 1 A of current is terminated linearly over 0.165 ms (also the time step used in our program). The comparison is quite good, with the late-time discrepancy reflecting a 10 percent difference in the time constant. Since the time constant of the body is about 2 ms, after 6 ms such a difference results in a 25 percent difference in the field values.

The geometric constraints placed on our current tubes do not allow for completely general eddy-current patterns. In particular, the current vortices are always centered on the axes of the body. For this reason, we do not expect our scheme to perform well for all geometries; a large (with respect to source and source-receiver geometry), shallow horizontal plate cannot be modeled accurately with our scheme.

Figure 7 shows a comparison of the secondary field decay for a cube in a 100 Ω · m half-space computed using our algorithm with an asymptotic sphere solution (Terry Lee, pers. comm.) for a coincident-loop array. The agreement appears quite good; however, we used a cube 90 m on a side, whereas a cube of the same volume as the sphere is just over 80 m on a side. The smaller cube results in a decay constant about 20 percent smaller. This discrepancy may be attributed, at least in part, to the difference in inductive responses of a cube and a sphere.

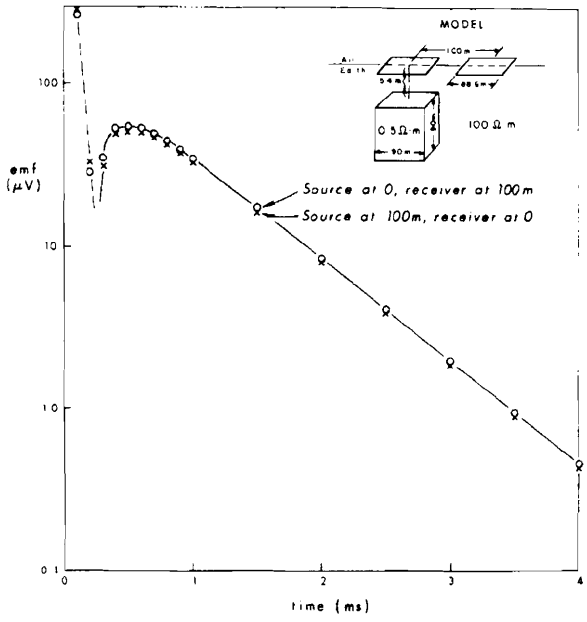

FIG. 5. Reciprocity check; dashed curve refers to negative response and solid curve to positive response.

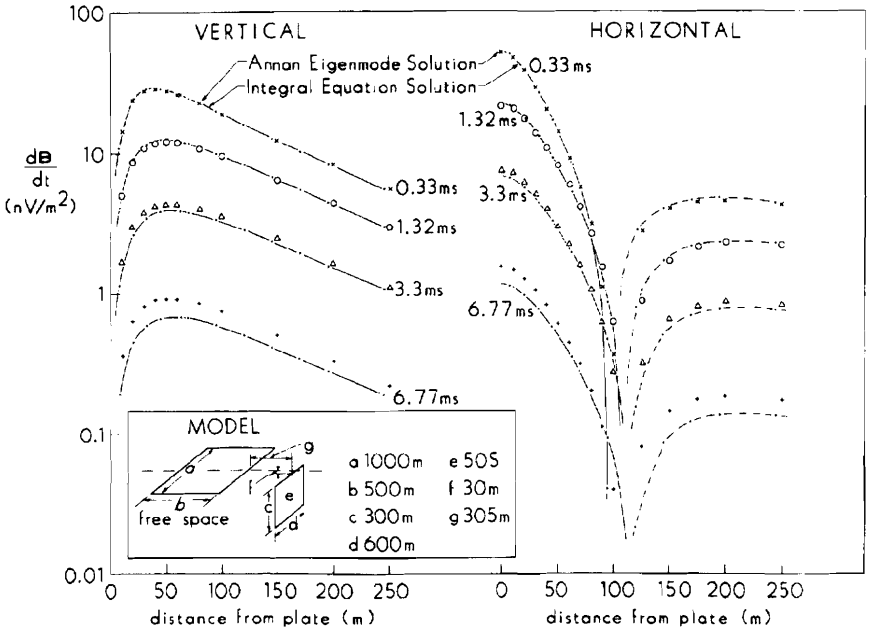

FIG. 6. Comparison of integral equation solution for a prism in free space (dashed curves for negative and solid curves for positive) with eigenmode thin-plate program for a large-loop array.

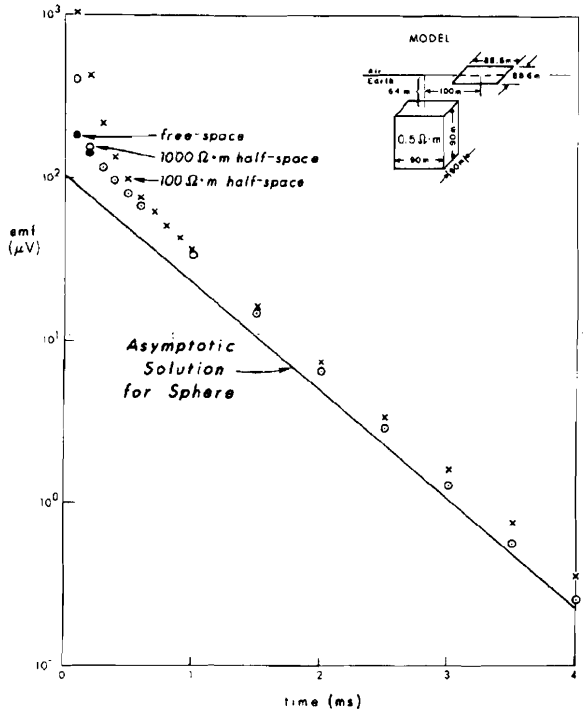

FIG. 7. Comparison of the secondary field response using a coincident loop system with an asymptotic sphere solution (T. Lee, pers. comm.) for a 0.5 Ω · m sphere of radius 50 m buried 100 m to center in a 100 Ω · m half-space. Also shown are the integral equation responses for the cube in a 1 000 Ω · m half-space and in free space. The free-space results coincide with the 1 000 Ω · m half-space results after the first two values.

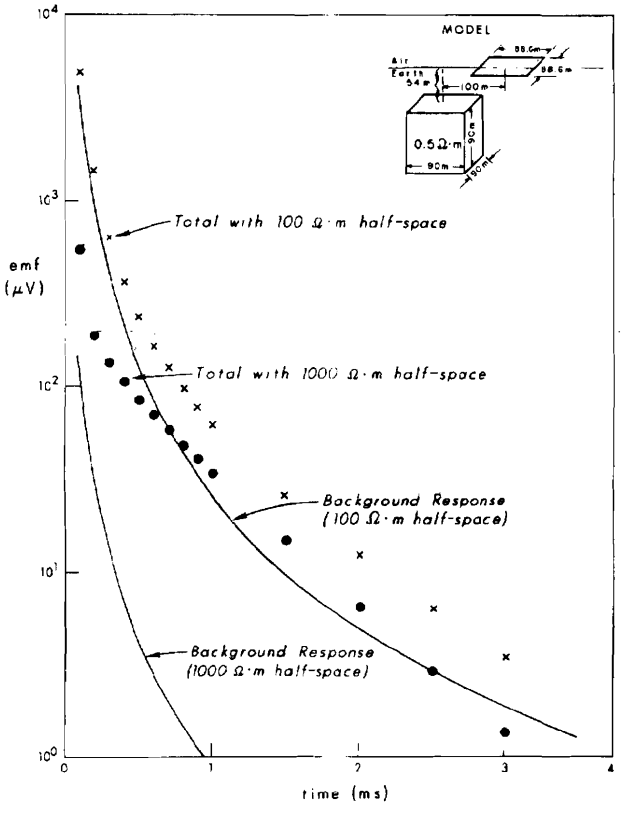

FIG. 8. Total and background (half-space) responses for the integral-equation solution models in Figure 7.

Figure 7 shows the effect of increasing the host resistivity from 100 Ω·m to 1 000 Ω·m and to the free-space limit. Current channeling is evident at early times, when the currents induced in the host are concentrated near the body. The secondary field is substantially greater than the free-space response at times earlier than 0.5 ms for the 100 Ω·m host, but with a 1 000 Ω·m host current channeling has disappeared by 0.1 ms. After 0.2 ms the secondary field of the body in a 1 000 Ω·m half-space is the same as that of the body in free space. Hence, simple superposition applies: the total response is the sum of the background (half-space) response and the response of the body in free space. However, for a 100 Ω·m half-space simple superposition only gives a rough approximation to the total response at late times.

The total and background responses for both the 100 Ω·m and 1 000 Ω·m half-space hosts are compared in Figure 8. Despite the enhanced secondary fields for the more conductive host, the larger background fields make the anomaly less detectable, and even though the secondary fields are approximately the same after 0.5 ms, the total fields are quite different.

As a final check, we transformed frequency-domain results using a refined version of the decay spectrum inversion technique introduced in Lamontagne (1975) and developed in Tripp (1982). The frequency-domain results were computed using the integral-equation solution described in Hohmann (1983) and Wannamaker et al. (1984), adapted for a large-loop source. The model (Figure 9) consists of a 600-m long, 20-m thick dike with 60-m depth extent and resistivity 1 Ω·m, buried 40 m in a 100 Ω·m half-space. The 600 m × 500 m transmitting loop is situated with its near side 300 m from the edge of the body, and a profile was computed across the center of the body at the Earth's surface, of the vertical and horizontal components of $d\mathbf{B}/dt$ at sample times 0.5, 1, 3, and 5 ms.

The profiles obtained from the inverse Fourier transformation are compared in Figures 9 and 10 with profiles from the direct time-domain integral-equation solution at sample times measured from both the top and bottom of the 0.125-ms current ramp. The agreement is excellent for both components. The anomaly in this example is virtually all due to current channeling (the secondary field decays as an inverse power of time rather than as an exponential at late times). The discretization used in the direct integral-equation solution consisted of 5 cells/quadrant in strike direction, and 6 cells in depth extent, 1 cell/quadrant thickness, and the individual cells were 6 subcells in strike length. This demonstrates the utility of noncubic cells (the computation cost for this model would be prohibitive without them). The discretization used in the frequency-domain program was quite different, with variable cell shapes used. Also, delta weighting functions were used. It is reassuring that the results are not sensitive to the choice of discretization or weighting functions. Total computer costs are about the same for the direct time-domain and inverse Fourier transformation methods. This particular model required about 2 hours of computer time on a Univac 1100/61 computer.

A comparison of the secondary fields and the free-space response (Figures 11 and 12) demonstrates that for this model the sum of the free-space and half-space fields does not approximate the total field. The free-space time constant for this model

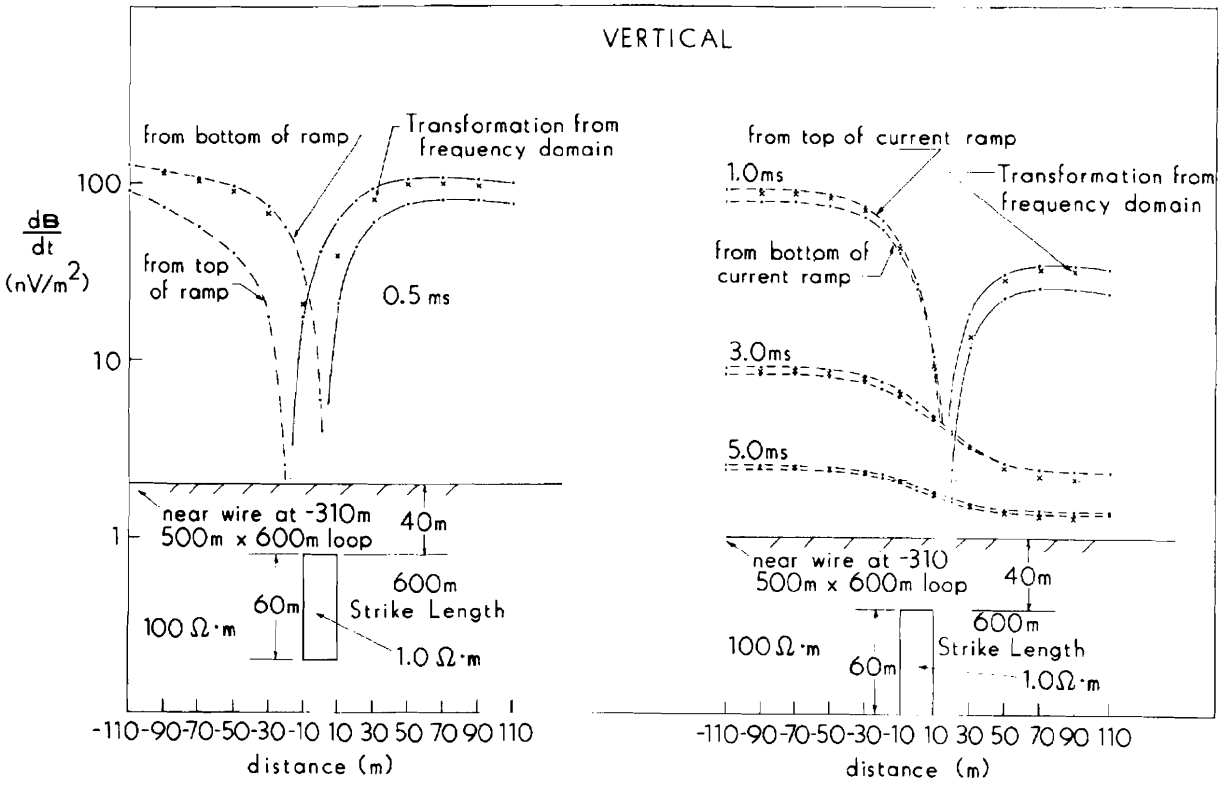

FIG. 9. Comparison of profiles for the vertical component of $d\mathbf{B}/dt$ calculated using the time-domain integral-equation solution, and by inverse Fourier transformation of frequency-domain integral-equation results. The ideal step response from the transformed data is compared with the direct time-domain calculations with time measured both from the top and from the bottom of the linear current ramp.

is less than 0.2 ms, whereas the time window during which half-space currents are concentrated in the vicinity of the body is a few milliseconds. Both the conductivity contrast and the geometry play a role in determining whether there is a time window during which the secondary field is similar to the free-space response.

CONCLUDING REMARKS

An integral equation for the transient electromagnetic (TEM) response of a confined region of anomalous conductivity in a conductive half-space can be formulated, and we have presented a numerical algorithm for a prismatic body. Although a matrix convolution of the time-domain tensor Green's function with all past values of the scattering current is required, the smoothing property of the integral operator allows for a large enough time step for the scheme to be practical.

In order to simulate the inductive response of a confined body (characterized by closed eddy currents), a specialized basis function subset must be included which satisfies the divergence-free boundary conditions so that the scalar potential term in the tensor Green's function drops out. Constructing such a set of basis functions in three dimensions is difficult without imposing geometric constraints that might prevent convergence to arbitrary current distributions, regardless of the level of discretization. However, the simple current-tube basis functions give reasonable approximations for models of moderate geometric extent. The same technique can, of course, be used in a frequency-domain integral equation solution.

We, and others who have worked on 3-D EM modeling in geophysics, have long been frustrated over the difficulty in obtaining a numerical algorithm that is satisfactory for a wide range of host conductivities. The addition of these basis functions has given us the best results to date. We emphasize, however, that we do not publish this technique as the final solution of the problem. We hope it will illuminate the nature of the problem and contribute to ideas of other researchers, leading to a more elegant scheme that treats the physics of the problem adequately.

ACKNOWLEDGMENTS

Valuable suggestions were made by Greg Steemson and Doug LaBrecque, and a discussion with Misac Nabighian provided important insight. We wish to thank Terry Lee for providing the sphere results, Peggy Gallagher for providing the thin-plate results, and Greg Newman for providing the Fourier-transformed 3-D results.

Financial support was provided by a consortium of private corporations including Amoco Production Co., ARCO Oil and Gas Co., Chevron Resources Company, Conoco, Inc., CRA Exploration Pty. Ltd., Sohio Petroleum Co., Union Oil Co. of

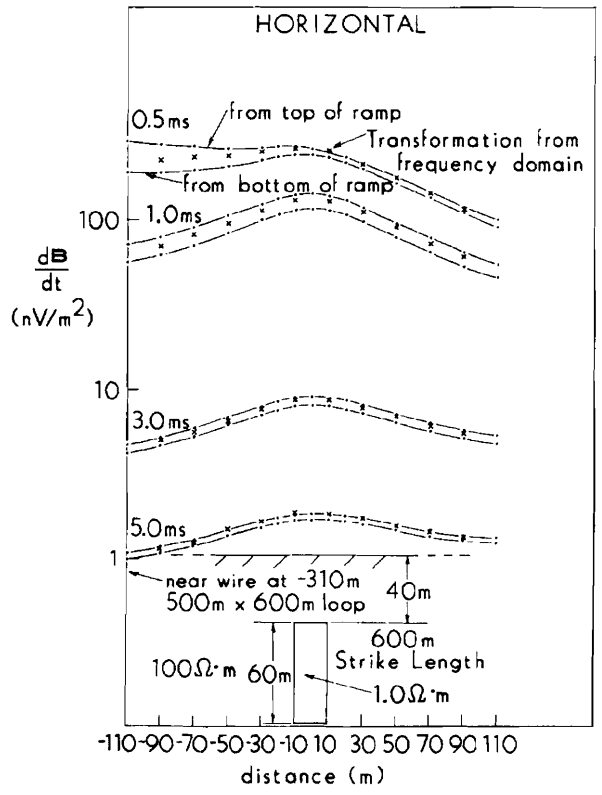

FIG. 10. Comparison of profiles for the horizontal component of total dB/dt calculated with the time-domain integral-equation solution, and by inverse Fourier transformation of frequency-domain integral-equation results.

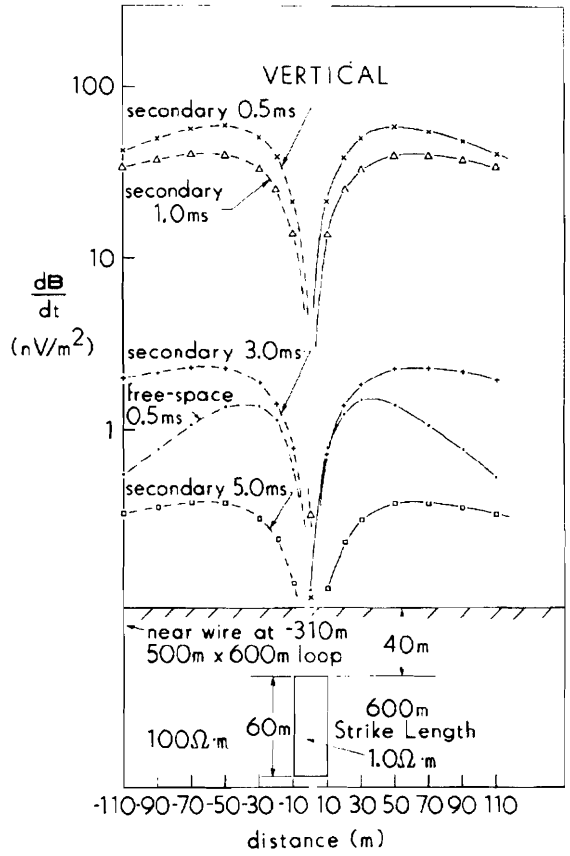

FIG. 11. Comparison of the vertical secondary field response for a body in a 100 Ω·m half-space with the response of the same body in free space. The latter is too small to be plotted at times later than 0.5 ms.

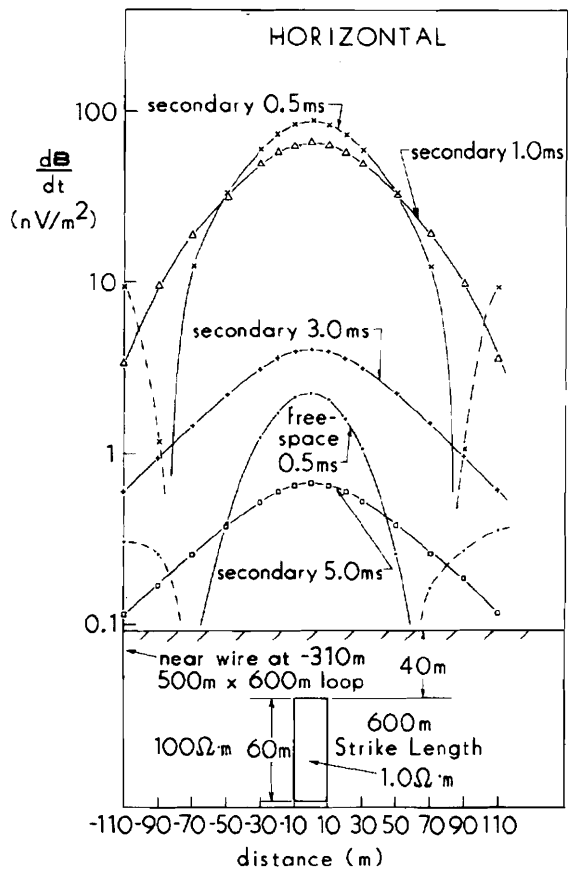

FIG. 12. Same as Figure 11, except horizontal magnetic field plotted.

California, and Utah International Inc., and also by U.S. Army Research Office Contract no. DAAG29-83-K-0012.

REFERENCES

Annan, A. P., 1974, The equivalent source method for electromagnetic scattering analysis and its geophysical application: Ph.D. thesis, Memorial Univ. of Newfoundland.

Goldman, M. M., and Stoyer, C. H., 1983, Finite-difference calculations of the transient field of an axially symmetric earth for vertical magnetic dipole excitation: Geophysics, **48**, 943–962.

Gradshteyn, I. S. and Ryzhik, I. M., 1965, Table of integrals, series, and products: Academic Press, Inc.

Harrington, R. F., 1968, Field computation by moment methods: The MacMillan Publishing Company.

Hohmann, G. W., 1975, Three-dimensional induced polarization and electromagnetic modeling: Geophysics, **40**, 309–324.

——— 1983, Three-dimensional EM modeling: Geophys. Surv., **6**, 27–53.

Kuo, J. T., and Cho, V.-H., 1980, Transient time-domain electromagnetics: Geophysics, **45**, 271–291.

Lajoie, J. J., and West, G. F., 1976, The electromagnetic response of a conductive inhomogeneity in a layered earth: Geophysics, **41**, 1133–1156.

Lamontagne, Y., 1975, Applications of wideband time-domain electromagnetic measurements in mineral exploration: Ph.D. thesis, Univ. of Toronto.

Lee, T. J., 1981, Transient electromagnetic response of a sphere in a layered medium: PAGEOPH, **119**, 309–338.

Nabighian, 1984, Forward and Introduction to Special Issue of GEOPHYSICS on time-domain electromagnetic methods of exploration: Geophysics, **49**, 849–853.

Oristaglio, M. L., and Hohmann, G. W., 1984, Numerical solution of Maxwell's equations in the time domain: Geophysics, **49**, 870–894.

Raiche, A. P., 1974, An integral equation approach to 3D modeling: Geophys. J. Roy. Astr. Soc., **36**, 363–376.

Tripp, A. C., 1982, Multi-dimensional electromagnetic modeling: Ph.D. thesis, Univ. of Utah.

Tripp, A. C., and Hohmann, G. W., 1984, Block diagonalization of the electromagnetic impedance matrix of a symmetric buried body using group theory: Inst. of Elect. and Electron. Eng. Trans. Geoscience and Remote Sensing, **GE-22**, 62–69.

Wannamaker, W. E., Hohmann, G. W., and SanFilipo, W. A., 1984, Electromagnetic modeling of three-dimensional bodies in layered earths using integral equations: Geophysics, **49**, 60–74.

Weidelt, P., 1975, Electromagnetic induction in three-dimensional structures: J. Geophys., **41**, 85–109.

——— 1983, The harmonic and transient electromagnetic response of a thin dipping dike: Geophysics, **48**, 934–952.